Published in final edited form as:

J Nucl Med. 2012 May ; 53(5): 779–786. doi:10.2967/jnumed.111.100073.

Molecular Imaging of Very Late Antigen–4 ($\alpha_4\beta_1$ Integrin) in the Premetastatic Niche

Monica Shokeen[1], **Alexander Zheleznyak**[1], **Jessica M. Wilson**[2], **Majiong Jiang**[2], **Ruiwu Liu**[3], **Riccardo Ferdani**[1], **Kit S. Lam**[3], **Julie K. Schwarz**[4], **Carolyn J. Anderson**[1,2,5,6]

[1]Mallinckrodt Institute of Radiology, Washington University, St. Louis, Missouri

[2]Department of Chemistry, Washington University, St. Louis, Missouri

[3]Department of Biochemistry and Molecular Medicine, UC–Davis Cancer Center, Sacramento, California

[4]Department of Radiation Oncology, Washington University, St. Louis, Missouri

[5]Department of Biochemistry and Molecular Biophysics, Washington University, St. Louis, Missouri

[6]Department of Radiology, University of Pittsburgh, Pittsburgh, Pennsylvania

Abstract

Despite advances in cancer treatment over the past few decades, metastatic disease remains the primary cause of morbidity and mortality. Recent reports suggest the formation of a "premetastatic niche" before the metastatic cascade, where *niche* is defined as the microenvironment for tumor cells to be able to engraft and proliferate at secondary sites. Bone marrow–derived (BMD) cells that express vascular endothelial growth factor receptor–1 and very late antigen–4 (VLA-4) have been shown to arrive at sites of metastasis to form a receptive environment for tumor cells. Here we describe experiments toward imaging of VLA-4–positive BMD cells using a high-affinity PET probe, ^{64}Cu-labeled 11-bis(carboxymethyl)-1,4,8,11-tetraazabicyclo[6.6.2] hexadecane (CB-TE2A)-LLP2A.

Methods: VLA-4–negative MDA-MB-231/firefly luciferase (*fluc*) human breast tumor cells were injected intraarterially in the left ventricle in nude mice. Tumor metastasis in mice was monitored for 30 d by bioluminescence imaging and small-animal PET/CT. Small-animal PET images were collected 2 h after mice were injected in the tail vein with ^{64}Cu-CB-TE2A-LLP2A (5.6–11.1 MBq [150–300 μCi; specific activity, 400 μCi/μg]). Cellular uptake of ^{64}Cu-CB-TE2A-LLP2A was determined in VLA-4–positive B16F10 mouse melanoma cells and VLA-4–negative MDA-MB-231/*fluc* human breast cancer tumor cells. Biodistribution experiments in nude mice bearing VLA-4–positive B16F10 subcutaneous tumors in the flank were conducted to validate targeting of VLA-4–positive cells in vivo.

For correspondence or reprints contact: Carolyn J. Anderson, Department of Radiology, University of Pittsburgh, 100 Technology Dr., Suite 452F, Pittsburgh, PA 15219. andersoncj@upmc.edu.

DISCLOSURE STATEMENT

The costs of publication of this article were defrayed in part by the payment of page charges. Therefore, and solely to indicate this fact, this article is hereby marked "advertisement" in accordance with 18 USC section 1734.

Results: Uptake of ^{64}Cu-CB-TE2A-LLP2A was higher in VLA-4–positive human melanoma B16F10 cells than in VLA-4–negative MDA-MB-231 cells ($P < 0.05$). In B16F10 tumor–bearing mice, ^{64}Cu-CB-TE2A-LLP2A had high uptake in the VLA-4–rich organs marrow, spleen, and tumor (11.26% ± 2.59%, 8.36% ± 2.15%, and 3.09% ± 0.58% injected dose/g, respectively). Cumulative standardized uptake value data from 2 independent studies ($n = 7$ and 8 mice) on nude mice implanted with VLA-4–negative MDA-MB-231/*fluc* human breast tumor cells suggested an influx of VLA-4–positive BMD cells that corresponded to metastasis ($P < 0.05$). Immunohistochemical analysis and flow cytometry also showed upregulation of VLA-4–positive cell clusters and BMD cells at the metastatic sites, providing evidence for noninvasive imaging of BMD cells in the premetastatic niche.

Conclusion: The results of the study demonstrated the potential of PET with VLA-4–targeted ^{64}Cu-CB-TE2A-LLP2A to visualize BMD cell reorganization and expansion noninvasively in vivo.

Keywords

very late antigen–4; premetastatic niche; ^{64}Cu; PET imaging

Despite the advances in cancer treatment over the past few decades, metastatic disease remains the primary cause of morbidity and mortality in cancer patients. Metastasis is a complex biologic process involving tumor cell intravasation, transport, and immune evasion within the circulatory system, arrest at a secondary site, extravasation, and finally colonization and growth (1). Each of these steps encounters physiologic barriers to the spread of malignant cells that must be overcome for tumor cells to successfully metastasize (2). Although dissemination of tumor cells is a prerequisite for metastasis, the 2 processes are not synonymous, since less than 1% of cancer cells entering the blood circulation successfully generate metastatic foci (3). Paget suggested over 100 y ago that a “congenial soil” promoted tumor growth at distant sites (4). Recent insights have suggested an additional step at the beginning of the metastatic cascade, the creation of a “premetastatic niche,” where *niche* is defined as the microenvironment for tumor cells to be able to engraft and proliferate at secondary sites (5). Here we describe experiments toward molecular imaging of bone marrow–derived (BMD) cells that putatively arrive before the implantation of the tumor cells at secondary sites. Imaging BMD cells in the premetastatic niche will provide a powerful diagnostic method that could enable intervention at a critical point in the cancer treatment process.

Circulating factors secreted by the primary tumor promote microenvironmental changes locally within the primary tumor and at distant sites. It has previously been reported that BMD cells expressing vascular endothelial growth factor receptor–1 (VEGFR-1) and very late antigen–4 (VLA-4, also known as integrin $\alpha_4\beta_1$) arrive at sites of metastasis and form a receptive environment for tumor cells (6). Kaplan et al. have shown that as early as 14 d after tumor implantation and, importantly, before tumor cell invasion, VEGFR-1–positive BMD hematopoietic progenitor cells (HPCs) were observed forming clusters at the sites of metastatic lesions (6). The study described VEGFR-1–positive cell clustering before tumor cell arrival in c-Myc transgenic mice, as well as in humans in “normal” tissue adjacent to the

primary site of metastasis, suggesting that the formation of VEGFR-1–positive HPC clusters may portend sites of future metastatic disease.

Peng et al. reported on a high-affinity peptidomimetic ligand, LLP2A (50% inhibitory concentration, 2 pM), against VLA-4 (7). They demonstrated that the biotin-conjugated LLP2A agent was taken up in VLA-4–expressing tumor-bearing mice and imaged by optical methods. LLP2A was also conjugated to 1,4,7,10-tetraazacyclododecane-*N,N′,N″,N‴*‴tetraacetic acid (LLP2A-DOTA) and labeled with ^{111}In (half-life, 67 h) for SPECT (single-photon CT) imaging, and this was compared with a ^{64}Cu-labeled (half-life, 12.7 h) LLP2A conjugated with 11-bis(carboxymethyl)-1,4,8,11-tetraazabicyclo[6.6.2] hexadecane (CB-TE2A), a highly stable Cu(II) chelator, for PET imaging applications (8). In the Raji lymphoma mouse model, there was ^{64}Cu-CB-TE2A-LLP2A uptake in the tumor, spleen, and bone marrow, all tissues that contain high levels of VLA-4. It was also shown that CB-TE2A-LLP2A expressed high affinity for Raji but not for VLA-4–negative HBT3477 cells (8).

In this study, we tested the hypothesis that ^{64}Cu-CB-TE2A-LLP2A is a PET radiopharmaceutical for imaging VLA-4–expressing BMD cells in sites of bone metastasis in a mouse model of human breast carcinoma. Results are reported for multimodality imaging experiments using bioluminescence imaging of firefly luciferase (*fluc*)–transfected, VLA-4–negative MDA-MB-231 tumor cells along with small-animal PET/CT of VLA-4–positive BMD cells using ^{64}Cu-CB-TE2A-LLP2A.

MATERIALS AND METHODS

Materials

All experiments involving the use of radioactive materials at Washington University were conducted under the authorization of the Radiation Safety Committee in accordance with the University's Nuclear Regulatory Commission license. ^{64}Cu (half-life, 12.7 h; β^+, 17.8%; $E_{\beta^+\,max}$, 656 keV; β_-, 38.4%; $E_{\beta^-\,max}$, 573 keV) was produced on a CS-15 biomedical cyclotron at Washington University School of Medicine (9). All chemicals were purchased from Sigma-Aldrich, unless otherwise specified, and solutions were prepared using ultrapure water (18 MΩ-cm resistivity). Radiochemistry reaction progress and purity were monitored by analytic reversed-phase high-performance liquid chromatography, which was performed on a Waters 600E chromatography system with a Waters 991 photodiode array detector and an Ortec model 661 radioactivity detector (EG&G Instruments). An Altima C18 Rocket column was used with a gradient that changes from 0.1% trifluoroacetic acid in water to 30:70 0.1% trifluoroacetic acid/water:0.1% trifluoroacetic acid/CH_3CN over the course of 5 min. Radioactive samples were counted using a Beckman 8000 automated well-type γ-counter. PET/CT data were acquired using either an Inveon Preclinical Imaging Station or a Focus 220 (Siemens Medical Solutions), and the CT images were acquired with an Inveon Preclinical Imaging Station. CB-TE2A was prepared as previously described (10).

Synthesis of CB-TE2A-LLP2A

CB-TE2A-LLP2A was prepared as previously described (8). The purity was determined to be greater than 95%. The identity of the compounds was confirmed by matrix-assisted laser desorption/ionization time-of-flight mass spectrometry (MALDI-TOF-MS) (MS [MH+], 1,723; theoretical, 1,723.97).

Radiolabeling of CB-TE2A-LLP2A with ^{64}Cu

^{64}Cu-chloride (5–10 μL in 0.5 M HCl) was diluted with 0.1 M ammonium acetate buffer (pH 8, 50–100 μL). The CB-TE2A-LLP2A solution (10 μg) was diluted with acetate buffer, ^{64}Cu-acetate (185 MBq [5 mCi]) was added, and the mixture was incubated at 80°C–95°C for 30–60 min. After purification, the radiochemical purity of the ^{64}Cu-labeled CB-TE2A-LLP2A was monitored by radio–high-performance liquid chromatography.

Cellular Uptake Assay

All cell handling was aseptically performed in a laminar flow hood. The MDA-MB-231 human breast cancer cell line was purchased from the American Tissue Culture Collection and was grown until 60%–75% confluent in T75 tissue culture flasks. The cells were maintained at a concentration of 1×10^6 cells/mL in Iscove modified Dulbecco medium (Gibco-BRL) at 37°C in a humidified atmosphere with 5% CO_2 in a Revco Elite II incubator. To determine cell density, equal amounts of cell suspension and trypan blue exclusion were added to a hemocytometer to calculate a cells/mL concentration and ensure cell viability.

Cell experiments were performed to determine the cellular uptake (sum of the internalized and cell surface–bound fractions) of ^{64}Cu-CB-TE2A-LLP2A in VLA-4–positive B16F10 mouse melanoma and VLA-4–negative MDA-MB-231/*fluc* human breast cancer tumor cells. Cells were grown in Iscove modified Dulbecco medium until 60%–75% confluent, were harvested by mechanical dissociation, and were resuspended in the binding medium (Iscove modified Dulbecco medium, 1% bovine serum albumin, and 1 mM Mn^{2+}) in microcentrifuge tubes. ^{64}Cu-CB-TE2A-LLP2A solution (1 nM) was added to the cell suspension. The samples were placed in a cell incubator for 60 min (37°C, 5% CO_2). To determine the in vitro targeting specificity of ^{64}Cu-CB-TE2A-LLP2A, samples were coincubated with 1 μM nonradioactive CB-TE2A-LLP2A solution (block) (500-μL total volume). After incubation, the samples were centrifuged at 1,400 rpm for 1 min, and the radioactive medium was removed. Cell pellets were rinsed with ice-cold binding buffer (500 μL) and centrifuged at 1,400 rpm for 1 min 2 times. The radioactivity in each fraction was measured in a well counter (Packard II γ-counter). The protein content of each cell lysate sample was determined (BCA protein assay kit; Pierce). The measured radioactivity associated with the cells was normalized to the amount of cell protein present (cpm/mg of protein).

Biodistribution Studies on B16F10 Tumor–Bearing Mice

All animal studies were performed according to the *Guide for the Care and Use of Laboratory Animals* (11) under the auspices of the Washington University Animal Studies Committee. B16F10 cells in phosphate-buffered saline were mixed 1:1 (v:v) with Matrigel

basement membrane matrix (Becton Dickinson), and 200 μL (1×10^7 cells) were injected subcutaneously into 5-wk-old C57BL/6 mice (Charles River Laboratories). The tumors were allowed to grow for 14–21 d (~619 [±261] mg), and the mice ($n = 5$ per group) were injected intravenously with 0.2 MBq (specific activity, 14.8 MBq/μg) of ^{64}Cu-CB-TE2A-LLP2A. The tumor-bearing mice were sacrificed 2 h later, and the blood, marrow, fat, heart, stomach, intestines, lungs, liver, spleen, kidneys, muscle, bone, pancreas, and tumor were harvested, weighed, and counted in the γ-counter. An additional group of mice was injected with ^{64}Cu-CB-TE2A-LLP2A premixed with an approximately 200-fold excess of LLP2A to serve as a blocking agent and were sacrificed at 2 h. The percentage injected dose per gram of tissue was determined by decay correction of the ^{64}Cu-labeled LLP2A for each sample normalized to a standard of known weight, which was representative of the injected dose.

Small-Animal Imaging Experiments

Bioluminescence imaging was performed to monitor the time course to metastasis in VLA-4–negative MDA-MB-231/*fluc* tumor cells injected intraarterially in the left ventricle. Mice were imaged once before tumor implantation (day 0). After the implantation of tumor cells (either intravenously or intradermally), the mice were imaged with bioluminescence imaging starting on day 4 after implantation and were followed by imaging 1–2 times per week until week 4. For bioluminescence imaging, the mice were injected intraperitoneally with a 150 mg/kg dose of D-luciferin (Biosynth) in phosphate-buffered saline, anesthetized with 2.5% isoflurane, and imaged with a charge-coupled device camera–based bioluminescence imaging system (IVIS 100; Caliper; exposure time, 1–5 min; binning, 16; field of view, 12; f/stop, 1; open filter). Signal was displayed as photons/s/cm^2/sr.

Before small-animal PET/CT, the mice were injected in the tail vein with ^{64}Cu-CB-TE2A-LLP2A (5.6–11.1 MBq [150–300 μCi; specific activity, 400 μCi/μg]). At 2 h after injection, the mice were anesthetized with 1%–2% isoflurane and imaged with small-animal PET, and the CT images were acquired with the Inveon. Static images were collected for 15 or 30 min and coregistered with Inveon Research Workstation software (Siemens Medical Solutions). PET images were reconstructed with the maximum a posteriori algorithm (12). The small-animal PET images were analyzed using ASIPro software, with 3–5 coronal slices of each leg using Inveon Research Workshop. Regions of interest were selected from PET images using CT anatomic guidelines, and the activity associated with them was measured with Inveon Research Workshop software. Three-dimensional regions of interest were drawn around the knee joint, through most of the tibia, and through the femur. Maximum standardized uptake values (SUVs) for both experiments were calculated using SUV = ([nCi/mL]×[animal weight (g)]/[injected dose (nCi)]).

Histology

Mouse leg bones were fixed in formalin, decalcified in 14% ethylenediaminetetraacetic acid, embedded in paraffin, and stained with hematoxylin and eosin (to visualize tumor cells) and for integrin α_4 (to visualize VLA-4–positive cells). Images were visualized under a Nikon Eclipse TE300 microscope equipped with a Plan Fluor 20/0.45 objective lens (Nikon) and a

Magnafire digital charge-coupled device camera according to a standard protocol using the Osteomeasure Analysis System software (Osteometrics).

Flow Cytometry

Total bone marrow was extracted from the femurs and tibias of tumor-bearing and tumor-naïve mice using a 25-gauge needle. Red cells were lysed in ammonium chloride–potassium lysis buffer. Residual cells were transferred to buffer (phosphate-buffered saline with 0.5% bovine serum albumin, 2 mM ethylenediamine tetraacetic acid, and 0.02% sodium azide), washed, filtered, and counted. Staining reactions were performed at 4°C in the presence of Fc block (clone 2.4G2; BD Biosciences) plus medium with serum. The following antibodies were purchased from eBio-science: PE-antimouse CD49 d (R1–2), rat IgG2b isotype control, APC-antimouse CD117 (c-Kit) (2B-8), mouse hematopoietic lineage biotin panel (antimouse CD3 (145–2C11), antimouse CD45R/B220 (RA3–6B2), antimouse CD11b (M1/70), antimouse erythroid marker (TER-119), and antimouse Ly06G (RB6–8C5). Streptavidin-PerCP was purchased from BD Biosciences. Flow cytometry was performed on FACSAria (BD Biosciences). α-4 (α_4)–positive HPCs were identified by gating the lineage-negative, *kit*-high population and referencing α-4 signal (PE) to matched isotype antibody control. HPC number is reported as the percentage of total marrow cells.

RESULTS

Radiochemistry

Radiochemical purity for ^{64}Cu-CB-TE2A-LLP2A was more than 95% as determined by radio–high-performance liquid chromatography. The specific activity for ^{64}Cu-CB-TE2A-LLP2A ranged from 11.1 to 14.8 MBq/μmol (300–400 μCi/μg).

Cellular Uptake of ^{64}Cu-CB-TE2A-LLP2A in MDA-MB-231/*fluc* Cells

To ensure that ^{64}Cu-CB-TE2A-LLP2A was binding to VLA-4 BMD cells and not to VLA-4–negative tumor cells, we used VLA-4–negative, *fluc*-transfected MDA-MB-231/*fluc* breast cancer cells to follow the timeline of metastasis in mice by bioluminescence imaging. MDA-MB-231/*fluc* cells were analyzed for surface expression of VLA-4 using flow cytometry. α-4 expression on B16F10 cells was used as the positive control. As shown in Figure 1A, MDA-MB-231/*fluc* tumor cells do not express VLA-4.

The cellular uptake (sum of the cell-internalized and cell surface–bound fractions) of ^{64}Cu-CB-TE2A-LLP2A in MDA-MB-231 cells and B16F10 cells is shown in Figure 1B. Cellular uptake was significantly less in MDA-MB-231 cells than in B16F10 cells ($P < 0.05$), and blocking with cold LLP2A was observed in B16F10 cells ($P < 0.05$), whereas there was no significant blocking in MDA-MB-231/*fluc* cells ($P = 0.3$). These data show that ^{64}Cu-CB-TE2A-LLP2A uptake in cells was by receptor-mediated endocytosis.

Biodistribution of ^{64}Cu-CB-TE2A-LLP2A in B16F10 Tumor-Bearing Mice

In vivo VLA-4 targeting of ^{64}Cu-CB-TE2A-LLP2A was validated in biodistribution experiments in nude mice bearing B16F10 subcutaneous tumors in the flank (Fig. 2A). The tumor-bearing mice were sacrificed 2 h after ^{64}Cu-CB-TE2A-LLP2A injection (185

kBq [5 μCi; specific activity, 400 μCi/μg]), organs of interest excised, and activity associated with those organs and tissues measured. The results indicated relatively high radiotracer uptake in the VLA-4–rich organs marrow and spleen (11.26% ± 2.59% and 8.36% ± 2.15% injected dose/g, respectively), and tumor uptake was 3.09% ± 0.58% injected dose/g. In a separate cohort of tumor-bearing mice, nonradioactive LLP2A ligand was coadministered with ^{64}Cu-CB-TE2A-LLP2A. The comparisons of the tumor-, spleen-, and marrow-to-blood ratios between the blocked and nonblocked mice were all statistically significant ($P < 0.05$), validating the in vivo VLA-4–targeting specificity of ^{64}Cu-CB-TE2A-LLP2A (Fig. 2B).

Serial Imaging of MDA-MB-231/*fluc* Mice by Bioluminescence Imaging and Small-Animal PET/CT

Bioluminescence imaging was conducted to monitor the time course of metastasis in the MDA-MB-231/*fluc* breast cancer mouse model. Mice were imaged once before tumor implantation (day 0). After the implantation of tumor cells, the mice underwent bioluminescence imaging starting on day 4 after implantation and then once weekly until week 4, or longer if possible. As expected, the bioluminescence signal from the tumors in leg bones increased over time for most animals. To correlate BMD cell signal with bone metastases, bioluminescence imaging was performed 1 d before the small-animal PET/CT session.

Small-animal PET/CT was conducted to assess whether ^{64}Cu-CB-TE2A-LLP2A could image VLA-4–positive BMD cells at the sites of metastatic disease. Figure 3A shows bioluminescence (top) and small-animal PET/CT (bottom) images of a representative mouse before and after implantation with MDA-MB-231/*fluc* cells. Images were obtained 3 d before tumor implantation (PET) and on days 3 (bioluminescence imaging), 4 (PET), 10 (bioluminescence imaging), and 11 (PET) after implantation. An additional bioluminescence image was obtained on day 18 and showed distinct tumor signals from both leg bones. Bone histology revealed a dense tumor mass in the left femur and a comparatively smaller tumor mass in the right femur (Fig. 3B). The SUV data from the small-animal PET image of the mouse demonstrated a significant increase ($P < 0.01$) in radiopharmaceutical uptake in both legs on day 11, compared with the uptake measured 3 d before tumor implantation (Fig. 3C). SUV increased from 0.053 to 0.084 (59%) in the right leg and from 0.046 to 0.085 (86%) in the left leg. Additionally, the SUV signal was about 1.5-fold higher in the left leg than in the right leg, and this difference correlated with the corresponding increase in bioluminescence signals. The cumulative data from 2 separate longitudinal imaging experiments showed that uptake of ^{64}Cu-CB-TE2A-LLP2A increased an average of 78% after tumor implantation (Figs. 3D and 3E). Taken together, these data demonstrated a 78% overall increase in uptake in the target organ (leg bone) after tumor implantation and a correlation between the uptake of ^{64}Cu-CB-TE2A-LLP2A and the appearance of MDA-MB-231 bone metastases on bioluminescence images.

Immunohistochemistry Validates the Presence of VLA-4–Positive Cells at Sites of Metastasis

The immunohistochemistry from a representative mouse (Figs. 4A and 4B) demonstrates that MDA-MB-231 cells do not express VLA-4 in vivo, whereas the bone marrow from a

mouse with bone metastases clearly shows clustering of VLA-4–positive cells (BMD cells) in areas that are distinct but proximal to MDA-MB-231 cell deposits. Similar clustering of the VLA-4–positive cells was not seen in the control mice (Fig. 4C).

Correlation Between Bioluminescence Imaging, Small-Animal PET/CT, and Flow Cytometry

Bioluminescence imaging/PET correlations tabulated in Figure 5 demonstrate that increased uptake of ^{64}Cu-CB-TE2A-LLP2A as measured by PET SUV correlated with increased bioluminescence signal in metastatic sites in the leg bones. Figure 5B shows the correlation between the normalized percentage of HPCs (corrected for the 1.7% HPCs found in normal mice) and the SUV of ^{64}Cu-CB-TE2A-LLP2A in the legs.

DISCUSSION

The goal of this work was to perform a proof-of-principle imaging study to address the feasibility of using the VLA-4–targeting PET radiopharmaceutical ^{64}Cu-CB-TE2A-LLP2A to monitor progression of metastasis manifested by the accumulation of VLA-4–positive BMD cells in the premetastatic niche in a mouse model of MDA-MB-231/*fluc* human breast cancer bone metastases. This radiotracer uses a high-affinity peptidomimetic ligand, LLP2A (50% inhibitory concentration, 2 pM) (7), against VLA-4 ($\alpha_4\beta_1$ integrin), which plays an important role in cancer metastasis (13). VLA-4 is a noncovalent heterodimeric transmembrane receptor that recognizes the QIDS (Gln-Ile-Asp-Ser) and ILDV (Ile-Leu-Asp-Val) motifs of 2 widely known ligands, the vascular cell adhesion molecule-1 (VCAM-1) and fibronectin, respectively (14,15). VLA-4 promotes the dissemination of tumor cells to distant organs by strengthening their adhesion to vascular endothelium and by facilitating tumor cell extravasation (16,17). Kaplan et al. showed that as early as 14 d after tumor implantation and, importantly, before tumor cell invasion, VEGFR-1–positive HPCs were observed forming clusters that dictated the sites of future metastatic lesions (6). Kaplan et al. described VEGFR-1–positive cell clustering before tumor cell arrival in c-Myc transgenic mice, as well as in “normal” human tissue adjacent to the primary site of metastasis, suggesting that the formation of VEGFR-1–positive clusters may portend sites of future metastatic disease (6,18). Along with the presence of VEGFR-1 in these premetastatic cell clusters, the interaction of VLA-4 on BMD cells with extracellular matrix fibronectin is essential for their migration within the bone marrow (19). Hiratsuka et al. reported that chemokines S100A8 and S100A9 increase expression of serum amyloid A3 in premetastatic lungs and that signaling through toll-like receptor 4 promotes accumulation of Mac1$^+$ myeloid cells at premetastatic sites (20). It is not clear at this time whether the presence of a primary tumor or lymph node involvement alters the expression of VEGFR-1 or VLA-4 in bone marrow–derived HPCs in the bone marrow or whether Mac1$^+$ myeloid cells also express VEGFR-1.

To our knowledge, there are no reports on imaging the process of premetastatic niche formation noninvasively in vivo. Toward this goal, we used PET/CT with ^{64}Cu-CB-TE2A-LLP2A (targeting VLA-4) supported by bioluminescence imaging, histology, and flow cytometry to monitor the development of the premetastatic niche in vivo. For this proof-of-concept study, we used VLA-4–negative human breast cancer cells (MDA-MB-231/*fluc*)

that form bone metastases in nude mice after intraarterial injection. Formation of metastases using this approach bypasses the formation of the primary tumor and, as such, may not accurately recapitulate the premetastatic environment. Future imaging studies will involve the use of alternate tumor models including subcutaneous and mammary fat pad injections to monitor the development of premetastatic sites.

Peng et al. evaluated the specificity of biotin-conjugated LLP2A to VLA-4 with cell-binding assays against different integrins using fluorescent microscopy and flow cytometry (7). Using histochemical staining and optical imaging, they showed strong binding of LLP2A-biotin to VLA-4–expressing cancer cells such as Molt-4 (acute lymphoblastic leukemia) cells, but no staining was observed on VLA-4–negative A549 (non–small cell lung cancer) cells, which express $\alpha_v\beta_1$, $\alpha_v\beta_3$, and $\alpha_3\beta_1$ integrins. Here, we performed cellular uptake assays (sum of the cell-internalized and cell surface–bound fractions) using the ^{64}Cu-CB-TE2A-LLP2A PET tracer in VLA-4–negative MDA-MB-231/*fluc* and VLA-4–positive B16F10 melanoma cells (confirmed by immunophenotyping, Fig. 1A). Uptake was found to be significantly less in MDA-MB-231/*fluc* cells than in B16F10 cells. Uptake of the radiotracer was blocked in the presence of excess nonradioactive ligand in B16F10 cells and had no impact on the MDA-MB-231/*fluc* cells. These data suggest that ^{64}Cu-CB-TE2A-LLP2A uptake is mediated by receptor VLA-4.

DeNardo et al. demonstrated targeting of ^{64}Cu-CB-TE2A-LLP2A in Raji lymphoma tumors in mice (8). Here we validated specific targeting of this tracer in VLA-4–positive B16F10 mouse melanoma tumors in C57/Bl6 mice (Fig. 2A). The data demonstrate higher tumor-, spleen-, and marrow-to-blood ($P < 0.05$) ratios in the nonblocked mice than in the blocked mice (Fig. 2B).

Small-animal PET/CT with ^{64}Cu-CB-TE2A-LLP2A supported by bioluminescence imaging was conducted to follow the timeline of tumor metastasis (bioluminescence imaging) and the presence of VLA-4–positive BMD cells (PET). Injected intraarterially, the MDA-MB-231/*fluc* human breast cancer cells caused bone metastasis in 2–3 wk, as demonstrated by bioluminescence imaging. Small-animal PET/CT was conducted to assess whether ^{64}Cu-CB-TE2A-LLP2A could image the accumulation of VLA-4–positive BMCs in response to tumor implantation. The data in Figures 3A–3E demonstrate that ^{64}Cu-CB-TE2A-LLP2A was capable of imaging the increase in VLA-4–positive BMD cells in target organs in response to tumor challenge. These data also showed a cumulative significant difference between tumor-naïve mice and mice several days after tumor implantation in 2 independent experiments. In Figure 3C, the PET signal was similar for both legs at day 4, but the bioluminescence imaging showed only 1 leg with a metastasis. However, the metastases eventually formed in both legs where the PET signal was high at day 11, demonstrating that the signal at day 4 may have been from VLA-4–positive metastatic cells. Even though the PET signal was low, it was quantifiable and was consistent between normal and tumor-bearing mice. Figure 4 validates the presence of α_4 in the bones of mice injected with tumor cells, but the α_4 was found not to be associated with, but rather to be proximal to, the tumor cells.

The relationship between bioluminescence photon flux, PET SUVs, and percentage of HPCs in the marrow by flow cytometry demonstrates that higher PET SUVs correlated with higher bioluminescence signal in the legs (Fig. 5A). The flow cytometry results suggest an expansion of lineage-negative, c-Kit–positive, α_4-positive cells in the bone marrow that is associated with the formation of bone metastasis. Our immunohistochemistry studies also suggest that BMD cells are reorganized into clusters proximal to α_4-integrin–negative tumor deposits (Fig. 4). These results are in keeping with preliminary results from Kaplan et al. that demonstrated ex vivo clustering of BMD HPCs in pre-metastatic sites in the lungs in animals with Lewis lung carcinoma or B16 primary tumors (6). In addition, there is a trend demonstrating a normalized percentage of HPCs versus SUV, where the normalized percentage of HPCs was corrected for the 1.7% found in normal, non–tumor-bearing mice in this study (Fig. 5B). Although the R^2 value was 0.35, the data demonstrated a trend toward increasing Uptake with an increasing percentage of HPCs. To our knowledge, our results are the first to document this phenomenon within the bone marrow itself in the context of a mouse model of bone metastasis.

Imaging of VLA-4–positive BMD HPCs within the bone marrow is typically more challenging because of the presence of resident normal bone marrow cells that are α_4-positive. These contribute to background signal for ^{64}Cu-CB-TE2A-LLP2A within the bone marrow (Fig. 3). In this study, we have used additional surface markers and flow cytometry to specifically quantify the BMD HPC population within the marrow and have initiated colony-forming assays to quantify progenitor cells. Future work will evaluate ^{64}Cu-CB-TE2A-LLP2A in premetastatic sites with fewer resident normal α_4-positive cells and lower background signal, such as the lung. Flow cytometry will be used to further characterize BMD cell populations that bind ^{64}Cu-CB-TE2A-LLP2A in premetastatic sites. Information on the colocalization of BMD cell populations and tumor cells will be obtained using immunofluorescence.

CONCLUSION

Here we have described PET with VLA-4–targeted ^{64}Cu-CB-TE2A-LLP2A to visualize BMD cell reorganization and expansion noninvasively in vivo. Successful imaging of the premetastatic niche has the potential to significantly improve patient outcomes by allowing for early identification and treatment of metastatic disease. ^{64}Cu-CB-TE2A-LLP2A could potentially be used for both imaging and therapy by delivering local radiation to sites of future metastatic disease. Studies in models that metastasize to sites other than bone are ongoing, and these will further validate our hypotheses and determine whether ^{64}Cu-CB-TE2A-LLP2A can be used for this purpose.

ACKNOWLEDGMENTS

We thank Michael Zahner for assistance with tissue culture studies, and Christopher Sherman, Nicole Fettig, Margaret Morris, and Lynn Collins for help with animal biodistribution and imaging experiments. We also thank David Piwnica-Worms for helpful discussions. This research was in part supported by funds from the U.S. NIH 5K 12HD00145910 and a Mary Kay Ash Charitable Foundation Grant in Innovative/Translational Research. Bioluminescence imaging was supported through NIH P50 CA94056. No other potential conflict of interest relevant to this article was reported.

REFERENCES

1. Yilmaz M, Christofori G, Lehembre F. Distinct mechanisms of tumor invasion and metastasis. Trends Mol Med. 2007;13:535–541. [PubMed: 17981506]
2. Geiger TR, Peeper DS. Metastasis mechanisms. Biochim Biophys Acta. 2009; 1796:293–308. [PubMed: 19683560]
3. Fidler IJ, Nicolson GL. Fate of recirculating B16 melanoma metastatic variant cells in parabiotic syngeneic recipients. J Natl Cancer Inst. 1977;58:1867–1872. [PubMed: 864765]
4. Paget S. The distribution of secondary growths in cancer of the breast. 1889. Cancer Metastasis Rev. 1989;8:98–101. [PubMed: 2673568]
5. Psaila B, Kaplan RN, Port ER, Lyden D. Priming the 'soil' for breast cancer metastasis: the pre-metastatic niche. Breast Dis. 2006–2007;26:65–74.
6. Kaplan RN, Riba RD, Zacharoulis S, et al. VEGFR1-positive haematopoietic bone marrow progenitors initiate the pre-metastatic niche. Nature. 2005;438: 820–827. [PubMed: 16341007]
7. Peng L, Liu R, Marik J, Wang X, Takada Y, Lam KS. Combinatorial chemistry identifies high-affinity peptidomimetics against $\alpha_4\beta_1$ integrin for in vivo tumor imaging. Nat Chem Biol. 2006;2:381–389. [PubMed: 16767086]
8. Denardo SJ, Liu R, Albrecht H, et al. ^{111}In-LLP2A-DOTA polyethylene glycol-targeting {alpha}4{beta}1 integrin: comparative pharmacokinetics for imaging and therapy of lymphoid malignancies. J Nucl Med. 2009;50:625–634. [PubMed: 19289419]
9. McCarthy DW, Shefer RE, Klinkowstein RE, et al. Efficient production of high specific activity 64Cu using a biomedical cyclotron. Nucl Med Biol. 1997;24:35–43. [PubMed: 9080473]
10. Sprague JE, Peng Y, Sun X, et al. Preparation and biological evaluation of copper-64-labeled tyr3-octreotate using a cross-bridged macrocyclic chelator. Clin Cancer Res. 2004;10:8674–8682. [PubMed: 15623652]
11. Guide for the Care and Use of Laboratory Animals. 8th ed. Washington, DC: National Academy Press; 2011.
12. Qi J, Leahy RM. Resolution and noise properties of MAP reconstruction for fully 3-D PET. IEEE Trans Med Imaging. 2000;19:493–506. [PubMed: 11021692]
13. Garmy-Susini B, Avraamides CJ, Schmid MC, et al. Integrin alpha4beta1 signaling is required for lymphangiogenesis and tumor metastasis. Cancer Res. 2010;70:3042–3051. [PubMed: 20388801]
14. Osborn L, Vassallo C, Browning BG, et al. Arrangement of domains, and amino acid residues required for binding of vascular cell adhesion molecule-1 to its counter-receptor VLA-4 (alpha 4 beta 1). J Cell Biol. 1994;124:601–608. [PubMed: 7508942]
15. Komoriya A, Green LJ, Mervic M, Yamada SS, Yamada KM, Humphries MJ. The minimal essential sequence for a major cell type-specific adhesion site (CS1) within the alternatively spliced type III connecting segment domain of fibronectin is leucine-aspartic acid-valine. J Biol Chem. 1991;266:15075–15079. [PubMed: 1869542]
16. Holzmann B, Gosslar U, Bittner M. Alpha 4 integrins and tumor metastasis. Curr Top Microbiol Immunol. 1998;231:125–141. [PubMed: 9479864]
17. Vincent AM, Cawley JC, Burthem J. Integrin function in chronic lymphocytic leukemia. Blood. 1996;87:4780–4788. [PubMed: 8639849]
18. Kaplan RN, Psaila B, Lyden D. Bone marrow cells in the 'pre-metastatic niche': within bone and beyond. Cancer Metastasis Rev. 2006;25:521–529. [PubMed: 17186383]
19. Hattori K, Heissig B, Wu Y, et al. Placental growth factor reconstitutes hematopoiesis by recruiting VEGFR1(1) stem cells from bone-marrow microenvironment. Nat Med. 2002;8:841–849. [PubMed: 12091880]
20. Hiratsuka S, Watanabe A, Aburatani H, Maru Y. Tumour-mediated upregulation of chemoattractants and recruitment of myeloid cells predetermines lung metastasis. Nat Cell Biol. 2006;8:1369–1375. [PubMed: 17128264]

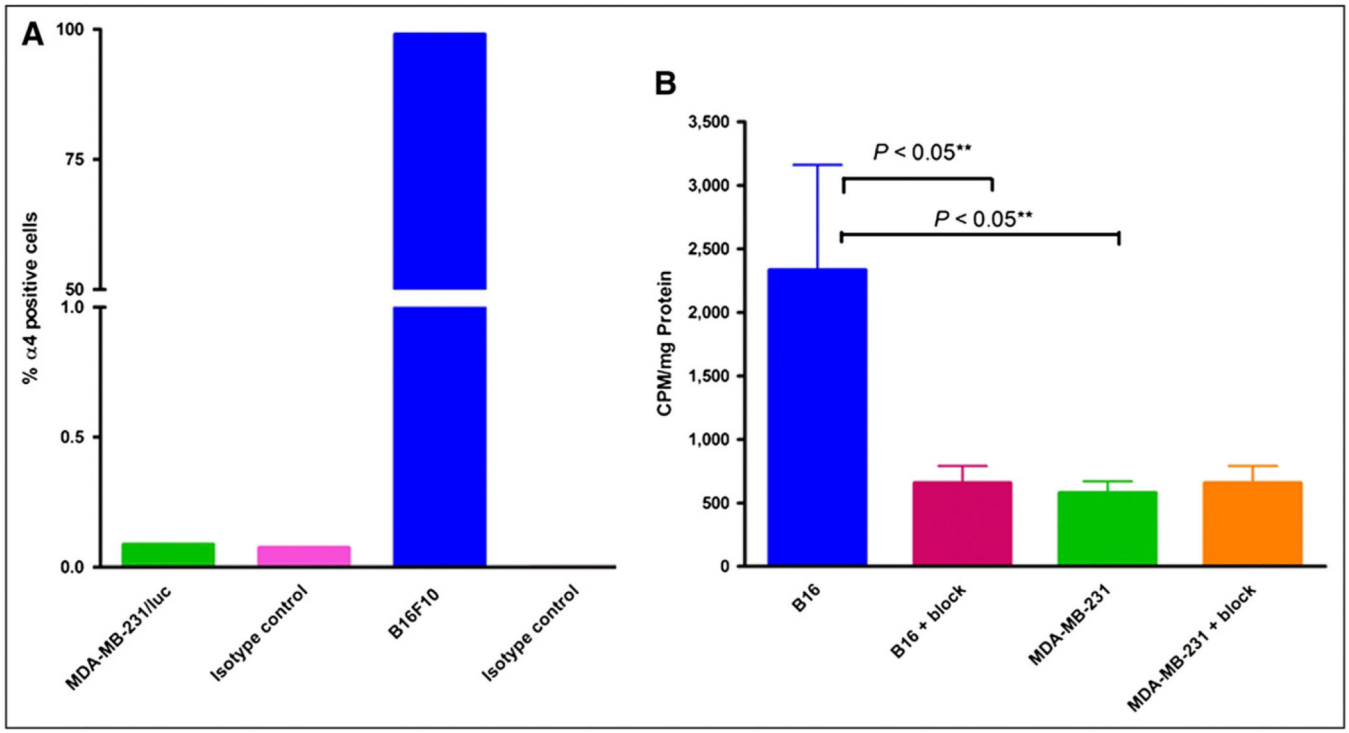

FIGURE 1.

(A) Percentage of α_4 (VLA-4)-positive cells in total tumor cell population as determined by flow cytometry. Bars represent flow data quantifying VLA-4 expression on tumor cells: MDA-MB-231/*fluc*, 0.088% (isotype control, 0.076%); B16F10, 99.08% (isotype control, 0.004%). (B) Cell-associated ^{64}Cu-CB-TE2A-LLP2A at 37°C at 60 min in VLA-4–positive B16F10 and VLA-4–negative MDA-MB-231 cells. Blocking was performed by coincubation with 1 μM nonradioactive LLP2A solution (500-μL total volume). Counts per minute (CPM) were normalized to milligrams of total protein present.

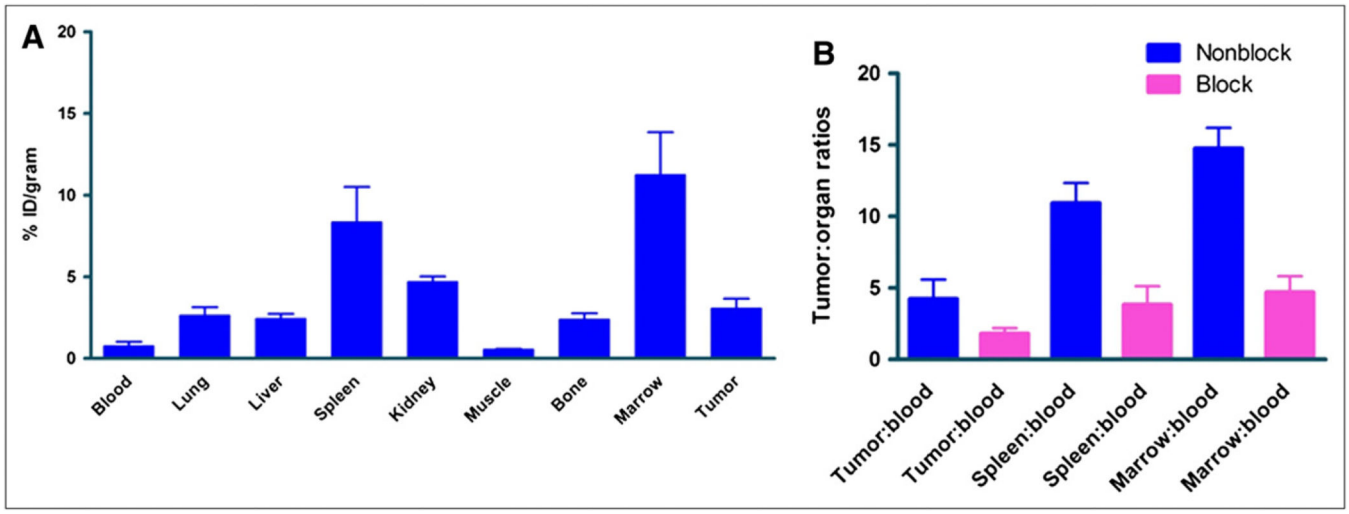

FIGURE 2.

(A) Biodistribution and tumor targeting of ^{64}Cu-CB-TE2A-LLP2A injected at 185 kBq (5 μCi; specific activity, 400 μCi/μg). Mice were sacrificed at 2 h after injection. (B) Comparison of key organs in presence and absence of block.

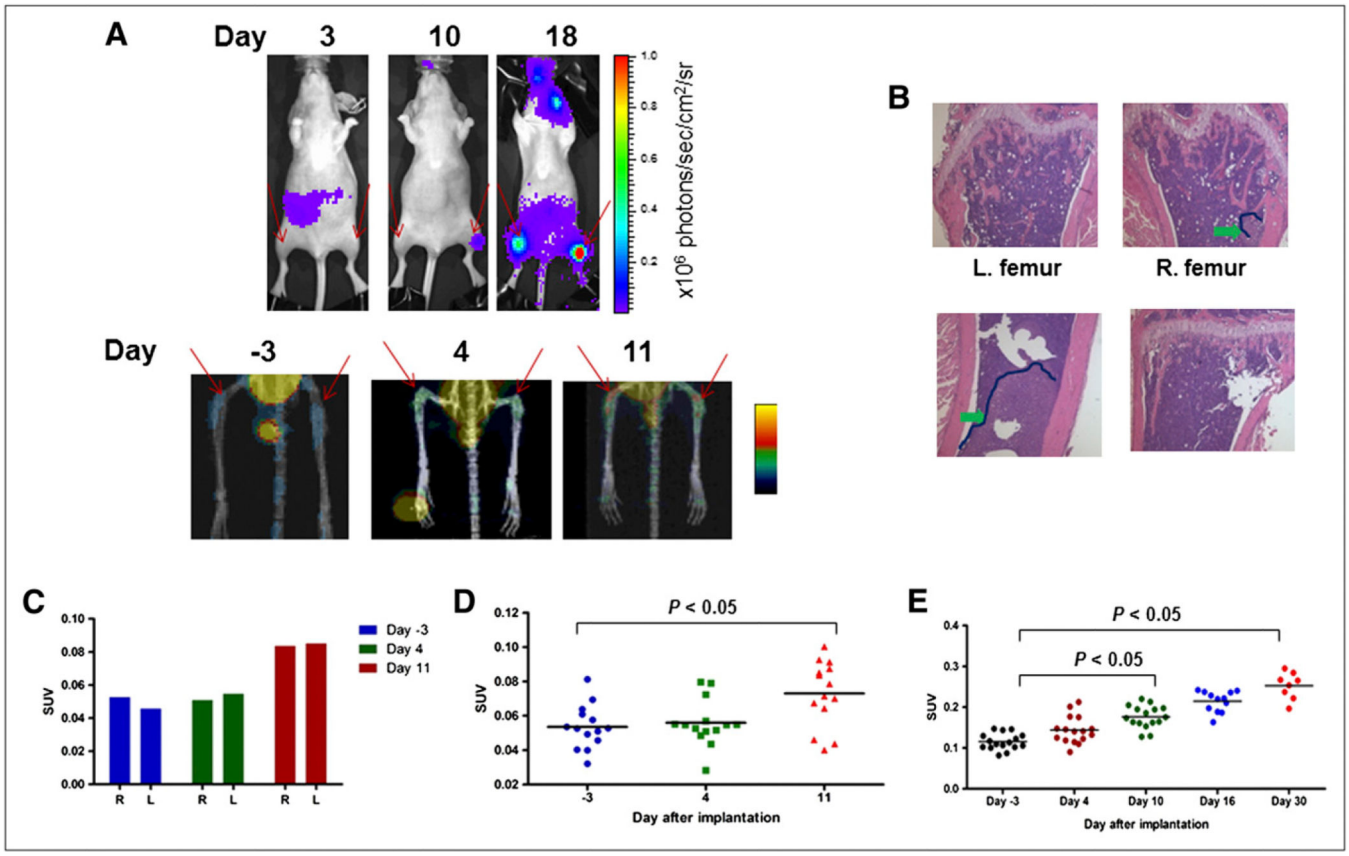

FIGURE 3.

Mice injected with MDA-MB-231/*fluc* intraarterially were monitored by bioluminescence imaging and small-animal PET/CT over time. Histology was performed to validate presence of tumors. (A) Bioluminescence imaging signal (top) and PET/CT (bottom) of representative mouse over time. Red arrows show sites of metastasis and tracer uptake. (B) Histology (hematoxylin and eosin staining) showing tumor lesions. Tumor area is outlined in dark blue. Lower tumor burden in right femur corresponded with lower SUV signal. (C) Cumulative leg SUV uptake in mouse shown in A. (D and E) Summary of cumulative leg SUV data collected in 2 independent tumor-bearing mouse experiments showing that uptake of ^{64}Cu-CB-TE2A-LLP2A in bone increases during time of metastasis. Tracer uptake in femurs was significantly higher at day 11 (D) and at days 10 and 30 (E) than at day −3 ($P < 0.05$).

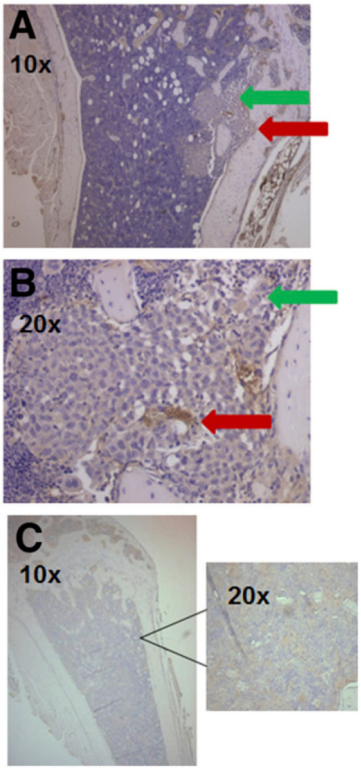

FIGURE 4.

Tumor cells are not $\alpha_4\beta_1$-positive. (A) Histologic sections of mouse leg bones stained with anti–α_4 antibody showing either tumor (green arrow) or $\alpha_4\beta_1$-positive HPC (red arrow). (B) Same slide at higher magnification. (C) Histologic section of bone from non–tumor-bearing mouse showing no staining from anti–α_4 antibody or at higher magnification.

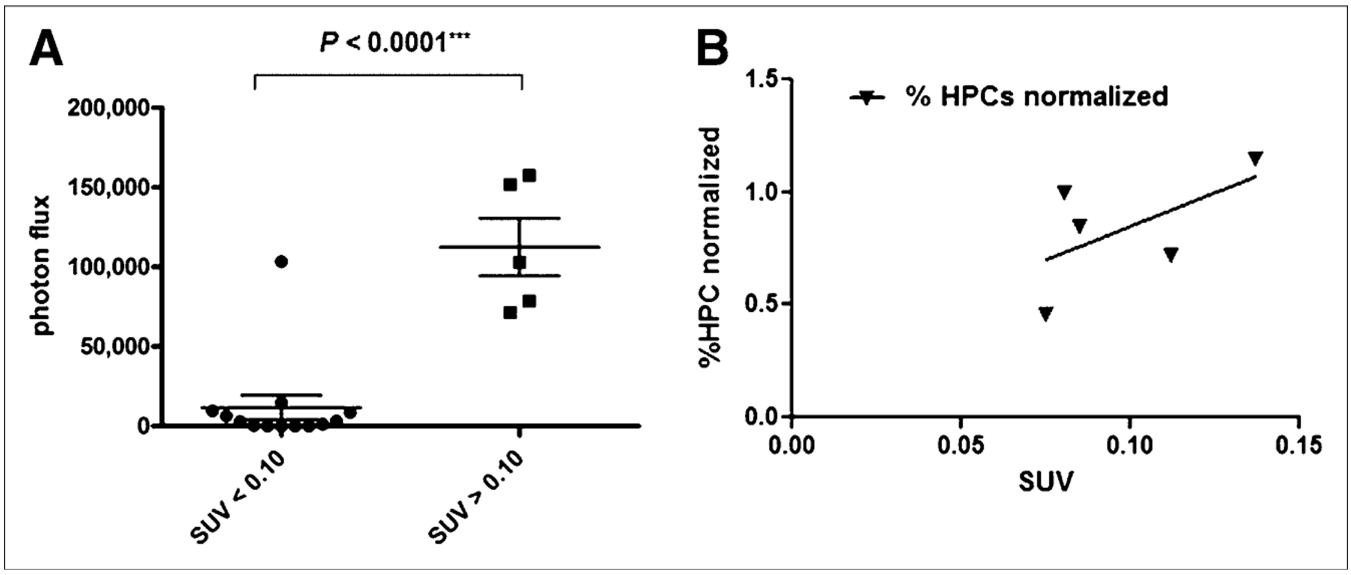

FIGURE 5.

(A) Bioluminescence imaging/PET correlation demonstrating that higher ^{64}Cu-CB-TE2A-LLP2A/PET SUVs correlated with higher bioluminescence imaging signal in legs. (B) Correlation between normalized percentage of HPCs (corrected for 1.7% HPCs found in normal mice) and SUV of ^{64}Cu-CB-TE2A-LLP2A in legs. Although $R^2 = 0.35$, data demonstrate trend showing increasing uptake with percentage of HPCs.